Yongliang Xiong* and Yifeng Wang

Uranyl oxalate species in high ionic strength environments: stability constants for aqueous and solid uranyl oxalate complexes

https://doi.org/10.1515/ract-2020-0083
Received August 9, 2020; accepted December 26, 2020;
published online January 22, 2021

Abstract: Uranyl ion, UO_2^{2+}, and its aqueous complexes with organic and inorganic ligands can be the dominant species for uranium transport on the Earth surface or in a nuclear waste disposal system if an oxidizing condition is present. As an important biodegradation product, oxalate, $C_2O_4^{2-}$, is ubiquitous in natural environments and is known for its ability to complex with the uranyl ion. Oxalate can also form solid phases with uranyl ion in certain environments thus limiting uranium migration. Therefore, the determination of stability constants for aqueous and solid uranyl oxalate complexes is important not only to the understanding of uranium mobility in natural environments, but also to the performance assessment of nuclear waste disposal. Here we developed a thermodynamic model for the UO_2^{2+}–Na^+–H^+–Cl^-–ClO_4^-–$C_2O_4^{2-}$–NO_3^-–H_2O system to ionic strength up to ~11 mol•kg^{-1}. We constrained the stability constants for $UO_2C_2O_4$(aq) and $UO_2(C_2O_4)_2^{2-}$ at infinite dilution based on our evaluation of the literature data over a wide range of ionic strengths up to ~11 mol•kg^{-1}. We also obtained the solubility constants at infinite dilution for solid uranyl oxalates, $UO_2C_2O_4$•$3H_2O$, based on the solubility data over a wide range of ionic strengths. The developed model will enable for the accurate stability assessment of oxalate complexes affecting uranium mobility under a wide range of conditions including those in deep geological repositories.

Keywords: disposal in salt formations; disposal in sedimentary basins; nuclear waste management; Pitzer model; reprocessing spent nuclear fuel.

***Corresponding author: Yongliang Xiong**, Department of Nuclear Waste Disposal Research & Analysis, Sandia National Laboratories (SNL), 1515 Eubank Boulevard SE, Albuquerque, NM 87123, USA, E-mail: yxiong@sandia.gov
Yifeng Wang, Department of Nuclear Waste Disposal Research & Analysis, Sandia National Laboratories (SNL), 1515 Eubank Boulevard SE, Albuquerque, NM 87123, USA, E-mail: ywang@sandia.gov

1 Introduction

Under oxidized conditions, uranium is mainly present in the +VI oxidation state. Therefore, uranyl ion, UO_2^{2+}, and its aqueous complexes with organic and inorganic ligands are the dominant species for the transport of naturally occurring uranium under oxidizing conditions. Consequently, they are important for the formation of uranium deposits and responsible for the movement of uranium in mine drainages and tailings related to uranium mining.

In the field of disposal of high-level nuclear waste (HLW) and spent nuclear fuel (SNF), uranyl ion and its aqueous complexes are expected to be important in at least two scenarios. First, in a deep geological disposal concept where spent nuclear fuel is disposed in oxidizing environments such as in an unsaturated zone, uranyl ion and its aqueous complexes are responsible for uranium mobilization. Second, even in a generally reducing disposal environment, a local oxidizing environment may be induced by radiolysis owing to radioactive decay within the long time scales of repository performance.

In natural environments, oxalate, $C_2O_4^{2-}$, is ubiquitous, as an important biodegradation product of humic and fulvic acids (e.g., [1]). Oxalate is known to form aqueous complexes with uranyl ion and thus facilitates uranium transport/mobility (e.g., [2]). In certain environments, oxalate can also form solid phases with uranyl ion, thus limiting the movement of uranium. Oxalate is also present in some nuclear waste streams. For instance, in the US nuclear waste management strategy, the oxalate concentrations for the Performance Assessment for Compliance Recertification Application in 2009 (CRA-2009) and 2014 (CRA-2014) for the Waste Isolation Pilot Plant (WIPP), the only operational geological repository currently in the world, were estimated to be 1.70×10^{-2} and 1.18×10^{-2} mol•dm^{-3}, respectively [3, 4]. In addition, in the French nuclear waste management programs, it has been demonstrated that radiolysis of bituminous nuclear wastes also produces oxalic acid, resulting in the formation of whewellite (CaC_2O_4•H_2O) [5], which is also a source of oxalate for the interactions with actinides in the near field of geological repositories.

The U(VI)-oxalate system was reviewed in the Nuclear Energy Agency (NEA) review series [6, 7]. The Specific Ion Interaction Theory (SIT) model was used for activity coefficient corrections for aqueous species. As the SIT model is generally valid to an ionic strength of up to ~3.5 mol•kg^{-1} [6], any application of those parameters to higher ionic strengths are considered beyond their validity range.

High ionic strength environments can be encountered in many nuclear waste applications, including deep geological nuclear waste disposal in sedimentary basins and salt formations, spent fuel reprocessing, and liquid nuclear waste treatment. In addition, evaporative conditions can also generate high ionic strength solutions in other rock formations for nuclear waste disposal. The brines in sedimentary basins in Canada considered for nuclear waste disposal have ionic strengths well beyond 3.5 mol•kg^{-1}. For instance, the brines in the Berea Formation in Devonian age in southern Ontario, Canada, considered for the nuclear waste disposal, have ionic strength up to 10.4 mol•kg^{-1} [8]. The brines in the salt formations at the WIPP, ERDA-6 (Energy Research and Development Agency Well 6) and GWB (Generic Weep Brine), have the ionic strengths of 5.82 and 8.26 mol•kg^{-1}, respectively [9]. The evaporator feed solutions for high-level waste processing at the Savannah River site contain both U(VI) and oxalate and have ionic strengths up to ~27 mol•kg^{-1} [10]. The aqueous feed solution in the co-decontamination step for the separation of U and Pu from fission products in reprocessing of spent fuel contains at least 4.2 mol•dm^{-3} HNO_3, 2.0 mol•dm^{-3} U(VI) and other elements with various concentrations [11], with a total stoichiometric ionic strength of at least 10.2 mol•dm^{-3}.

The above examples illustrate the need for development and establishment of a thermodynamic model for U(VI)-oxalate systems valid beyond the limit of the SIT model. Since the Pitzer model can be applied to high ionic strengths up to the saturation of most salts, in this study we will develop a Pitzer model for the system of UO_2^{2+}–Na^+–H^+–Cl^-–ClO_4^-–$C_2O_4^{2-}$–NO_3^-–H_2O. We will then perform the validation tests by comparing the model predictions with the model-independent experimental results. Finally, we will provide an example for model application.

2 Method

In this study, the standard state for a solid phase is defined as its pure end-member with unit activity at a temperature and pressure of interest. The standard state of the solvent in aqueous solutions is pure solvent at the temperature and pressure of interest. The standard state for an aqueous solute is a hypothetical one molal (mol•kg^{-1}) solution of infinite dilution at the temperature and pressure of interest.

The computer code EQ3/6 Version 8.0a [12, 13] is employed as the modeling platform, and the parameters for uranyl-oxalate speciation are listed in Table 1. The goal of the modeling is to minimize the difference between experimental data and model predictions. A similar modeling approach can be found in our previous work (e.g., [14–16]).

In our model development, we rely on the Pitzer model for the dissociation of oxalic acid developed by Thakur et al. [17] as well as the Pitzer parameters for UO_2^{2+}–Cl^-, UO_2^{2+}–ClO_4^-, and UO_2^{2+}–NO_3^- from previous studies [18, 19] (see Table 1). In Thakur et al. [17], the dissociation constants of oxalic acid were determined via potentiometric method. The titrations were performed at low total oxalate concentrations and mostly in acidic pH without any precipitation. We first evaluate the stability constants for $UO_2C_2O_4$(aq) and $UO_2(C_2O_4)_2^{2-}$ along with the associated Pitzer parameters. Similarly, we evaluate the solubility constants for U(VI)-oxalate solid phases such as $UO_2C_2O_4$•$3H_2O$, based on the stability constants for $UO_2C_2O_4$(aq) and $UO_2(C_2O_4)_2^{2-}$ with associated Pitzer parameters.

The first step is to generate EQ3/6 modeling input files using experimental data. In the second step, the target parameter values (e.g., log K) are adjusted by minimizing the difference between experimental values (e.g., $\log_{10}\beta^I_{101}$, or $\log_{10}\beta^I_{102}$, or $m_{\sum U(VI)}$) and model predictions through the use of a computer code. In the third step, the final selected value for the targeted parameter is validated by independent experimental data. The uncertainties reported in this study are two standard deviations (2σ). Error propagations are calculated based on uncertainties associated with regressions and equilibrium constants in the model.

The experimental data used in our analyses of stability constants for $UO_2C_2O_4$(aq) and $UO_2(C_2O_4)_2^{2-}$ include [20–32]. These experimental data were obtained predominantly in a $NaClO_4$ medium. The experimental data from Choppin et al. [26] and Crea et al. [29] were obtained in a NaCl medium. Experimental data from Choppin et al. [22] are for mixtures of HNO_3 and $NaNO_3$. The room temperature experimental data from Leturcq et al. [33] for the solubility of $UO_2C_2O_4$•$3H_2O$(cr) was conducted in a mixture of $H_2C_2O_4$ and HNO_3 solutions and used in this study to model the solubility constant of this solid.

3 Results

In this study, the stability constants for $UO_2C_2O_4$(aq) and $UO_2(C_2O_4)_2^{2-}$ at a given ionic strength are expressed as $\log_{10}\beta^I_{101}$ and $\log_{10}\beta^I_{102}$, respectively, corresponding to the following equations,

$$UO_2^{2+} + C_2O_4^{2-} \rightleftharpoons UO_2C_2O_4(aq) \quad (1)$$

$$\beta^I_{101} = \frac{m_{UO_2C_2O_4(aq)}}{m_{UO_2^{2+}} \times m_{C_2O_4^{2-}}} \quad (2)$$

$$UO_2^{2+} + 2C_2O_4^{2-} \rightleftharpoons UO_2(C_2O_4)_2^{2-} \quad (3)$$

$$\beta^I_{102} = \frac{m_{UO_2(C_2O_4)_2^{2-}}}{m_{UO_2^{2+}} \times \left(m_{C_2O_4^{2-}}\right)^2} \quad (4)$$

where m_i denotes the concentration of the ith species on a molal scale, mol•kg^{-1}.

Table 1: Thermodynamic model with the Pitzer formalism for the UO_2^{2+}–Na^+–H^+–Cl^-–ClO_4^-–$C_2O_4^{2-}$–NO_3^-–H_2O system at 25 °C.

Pitzer binary interaction parameters				
Interactions	$\beta^{(0)}$	$\beta^{(1)}$	C^{ϕ}	**Reference**
UO_2^{2+}–Cl^-	0.4274	1.644	−0.0184	[19]
UO_2^{2+}–ClO_4^-	0.61133	2.14425	0.02164	[18]
UO_2^{2+}–NO_3^-	0.46072	1.61325	−0.03150	[18]
Na^+–$HC_2O_4^-$	−0.2886	0.29	0.068	[17]
Na^+–$C_2O_4^{2-}$	−0.2770	1.74	0.122	[17]
Na^+–$UO_2(C_2O_4)_2^{2-}$	−1.0368	1.74	0.3646	This work
Pitzer ternary interaction parameters involving neutral species				
Interactions			ζ	Reference
Na^+–Cl^-–$UO_2C_2O_4$(aq)			−0.08479	This work
Na^+–ClO_4^-–$UO_2C_2O_4$(aq)			0.09149	This work
Na^+–NO_3^-–$UO_2C_2O_4$(aq)			−0.08100	This work
Pitzer mixing parameters				
Interactions			θ	Reference
ClO_4^-–$UO_2(C_2O_4)_2^{2-}$			0.1148	This work
H^+–UO_2^{2+}			0.2730	This work
Equilibrium constants				
Reaction			log K	Reference
$H_2C_2O_4$(aq) = $2H^+ + C_2O_4^{2-}$			−6.07	[17]
$HC_2O_4^- = H^+ + C_2O_4^{2-}$			−4.36	[17]
$UO_2^{2+} + C_2O_4^{2-} = UO_2C_2O_4$(aq)			7.54 ± 0.30	This work
$UO_2^{2+} + 2C_2O_4^{2-} = UO_2(C_2O_4)_2^{2-}$			11.57 ± 0.20	This work
$UO_2C_2O_4 \bullet 3H_2O$(cr) = $UO_2^{2+} + C_2O_4^{2-} + 3H_2O$(l)			−9.35 ± 0.25	This work

The corresponding stability constants at infinite dilution are expressed as $\log_{10}\beta^0_{101}$ and $\log_{10}\beta^0_{102}$,

$$\beta^0_{101} = \beta^I_{101} \times \frac{\gamma_{UO_2C_2O_4(aq)}}{\gamma_{UO_2^{2+}} \times \gamma_{C_2O_4^{2-}}} \quad (5)$$

$$\beta^0_{102} = \beta^I_{102} \times \frac{\gamma_{UO_2(C_2O_4)_2^{2-}}}{\gamma_{UO_2^{2+}} \times \left(\gamma_{C_2O_4^{2-}}\right)^2} \quad (6)$$

where γ_i denotes the activity coefficient of the ith species.

The solubility constant for $UO_2C_2O_4 \bullet 3H_2O$(cr) at a certain ionic strength ($\log_{10}K^I_{sp}$) is expressed as,

$$UO_2C_2O_4 \bullet 3H_2O(cr) \rightleftharpoons UO_2^{2+} + C_2O_4^{2-} + 3H_2O(l) \quad (7)$$

$$K^I_{sp} = m_{UO_2^{2+}} \times m_{C_2O_4^{2-}} \quad (8)$$

The corresponding solubility constant at infinite dilution should be

$$K^0_{sp} = K^I_{sp} \times \gamma_{UO_2^{2+}} \times \gamma_{C_2O_4^{2-}} \times (a_{H_2O})^3 \quad (9)$$

where a_{H_2O} is the activity of water at the corresponding ionic strength.

The model parameters developed in this study are tabulated in Table 1. Our model include the stability constants for $UO_2C_2O_4$(aq) and $UO_2(C_2O_4)_2^{2-}$, and the solubility constant for $UO_2C_2O_4 \bullet 3H_2O$(cr) as well as a series of Pitzer parameters. The Pitzer zeta parameters (ζ_{ijk}) for Na^+–Cl^-–$UO_2C_2O_4$(aq), Na^+–ClO_4^-–$UO_2C_2O_4$(aq), and Na^+–NO_3^-–$UO_2C_2O_4$(aq) plus the retrieval of $\log_{10}\beta^0_{101}$ are obtained through regression of experimental data used to compute $\log_{10}\beta^I_{101}$ for $UO_2C_2O_4$(aq) in NaCl, $NaClO_4$ and HNO_3 + $NaNO_3$ mixtures. Similarly, the binary interaction parameters for Na^+–$UO_2(C_2O_4)_2^{2-}$ and the mixing parameter (θ_{ij}) for ClO_4^-–$UO_2(C_2O_4)_2^{2-}$, as well as $\log_{10}\beta^0_{102}$, are computed through regression of experimental data for $\log_{10}\beta^I_{102}$ of $UO_2(C_2O_4)_2^{2-}$ in NaCl and $NaClO_4$. The mixing parameter (θ_{ij}) for the H^+–UO_2^{2+} interaction as well as the $\log_{10}K^0_{sp}$ for $UO_2C_2O_4 \bullet 3H_2O$(cr) were computed using the experimental solubility data for $UO_2C_2O_4 \bullet 3H_2O$(cr) in $H_2C_2O_4$ and HNO_3 solution mixtures.

Figure 1 illustrates the predicted stability constants for $UO_2C_2O_4$(aq) as a function of ionic strength up to ~11 mol•kg^{-1} in comparison with the experimental results. The experimental results are in NaCl and $NaClO_4$ solutions. The comparison indicates that the model performs well over a wide range of ionic strengths in both NaCl-bearing and $NaClO_4$-bearing media. It may be of interest to note that the experimental data, especially those in NaCl solutions, scatter to some degrees. In the NEA review, those data in NaCl solutions were corrected for the complexation with chloride [6]. The complexation of

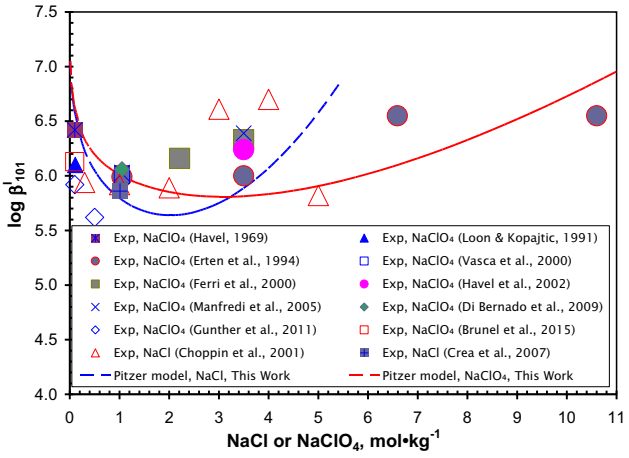


Figure 1: Comparison of the stability constants for $UO_2C_2O_4(aq)$ as a function of ionic strength in NaCl and $NaClO_4$ media predicted by the model with the experimental data. The symbol size is similar to the experimental uncertainties, which also applies other figures hereafter.

UO_2^{2+} with chloride is not considered in our model. Instead, the effect of chloride is absorbed by the interactions of UO_2^{2+}–Cl^- and Na^+–Cl^-–$UO_2C_2O_4(aq)$ in our model (Table 1).

In Table 2, the predicted stability constants for $UO_2C_2O_4(aq)$ in the mixture of HNO_3 and $NaNO_3$ are compared with the experimental results from Choppin et al. [22]. The original experimental results are in molarity units, mol•dm^{-3}. In this study, the stability constants in molarity units are converted to those in molality units, according to the following equation,

$$\log_{10}\beta^I_{101,m} = \log_{10}\beta^I_{101,M} + \sum_i \upsilon_i \times \log_{10} Q \qquad (10)$$

where $\log_{10}\beta^I_{101,m}$ is the stability constant in molality units. $\log_{10}\beta^I_{101,M}$ stands for the stability constant in molarity units and $\sum_i \upsilon_i$ represents the summation of stoichiometric coefficients in Eq. (1). Q denotes the conversion factor from molarity to molality concentration units. For pure HNO_3, the conversion factor is calculated based on the density for HNO_3 solutions from [34]. For mixtures of HNO_3 and $NaNO_3$, the conversion factors are calculated from the densities of the mixtures. These densities of mixtures are computed based on the method of [35, 36] for the prediction of thermodynamic properties, including densities, of mixtures, according to the densities of their pure constituent components. In this case, the densities for pure HNO_3 and $NaNO_3$ are taken from [34].

Notice that Hummel et al. [6] also evaluated the stability constant for $UO_2C_2O_4(aq)$ in pure HNO_3 from Choppin et al. [22]. They considered the association of UO_2^{2+} with NO_3^- [6]. Therefore, their final $\log_{10}\beta^I_{101,m}$ in 4.57 mol•kg^{-1} HNO_3 was 7.25 after the correction of the association of UO_2^{2+} with NO_3^-, and the conversion from molar units to molal units. Their value (i.e., 7.25) is quite different from the original value of 6.36 for $\log_{10}\beta^I_{101,M}$ from Choppin et al. [22]. In contrast, our converted and model-predicted $\log_{10}\beta^I_{101,m}$ values of 6.53 and 6.22 (Table 2), respectively. The difference between our value and that from Hummel et al. (2005) can be attributed to the fact that our model considers that the electrolyte of $UO_2(NO_3)_2$ is fully dissociated. The effect of nitrate is absorbed by the interaction of UO_2^{2+}–NO_3^- in our model. In Choppin et al. [22], no association of UO_2^{2+} with NO_3^- was considered by the authors either. Also, notice that Hummel et al. [6] did not evaluate all stability constants from Choppin et al. (1983) [22] in the mixtures of HNO_3 and $NaNO_3$. We have, in addition, evaluated all stability constants from Choppin et al. [22] in HNO_3 and $NaNO_3$ mixtures. These stability constant values are consistent with those in pure HNO_3 (see Table 2). Our model-predicted values agree with the experimental values within the associated uncertainties.

Figure 2 shows the comparison of the model-predicted stability constants for $UO_2(C_2O_4)_2^{2-}$ as a function of ionic

Table 2: Comparison of the model-predicted stability constants for $UO_2C_2O_4(aq)$ in the mixtures of HNO_3 and $NaNO_3$ with the experimental data from Choppin et al. [22].

Media, molar scale	$\log\beta^I_{101}$, molar scale	Media, molal scale	$\log\beta^I_{101}$, molal scale	$\log\beta^I_{101}$, molal scale, model	Diff.
4 mol•dm^{-3} HNO_3 + 0 mol•dm^{-3} $NaNO_3$	6.36	4.57 mol•kg^{-1} HNO_3 + 0 mol•kg^{-1} $NaNO_3$	6.53	6.22	−0.31
3 mol•dm^{-3} HNO_3 + 1 mol•dm^{-3} $NaNO_3$	6.26	3.67 mol•kg^{-1} HNO_3 + 1.22 mol•kg^{-1} $NaNO_3$	6.52	6.38	−0.14
2 mol•dm^{-3} HNO_3 + 2 mol•dm^{-3} $NaNO_3$	6.22	2.57 mol•kg^{-1} HNO_3 + 2.57 mol•kg^{-1} $NaNO_3$	6.55	6.56	0.01
1 mol•dm^{-3} HNO_3 + 3 mol•dm^{-3} $NaNO_3$	6.20	1.29 mol•kg^{-1} HNO_3 + 3.86 mol•kg^{-1} $NaNO_3$	6.53	6.65	0.12

strength with the experimental results. The experimental results are in NaCl and $NaClO_4$ media. The model is valid up to ~11 mol•kg^{-1}. The model performs well in both NaCl and $NaClO_4$ media over a wide range of ionic strengths.

In Figure 3, the model-predicted values for the solubility of $UO_2C_2O_4$•$3H_2O$(cr) in the mixtures of $H_2C_2O_4$ and HNO_3 are compared with the experimental results from Leturcq et al. [13]. Notice that the experimental results from [33] at room temperature are used in our model development. The original solute concentration data from [33] are in molarity units. In this study, we convert these to molality units. In the concentration conversion, we first calculate the densities for the $H_2C_2O_4$ and HNO_3 mixture. Similarly,

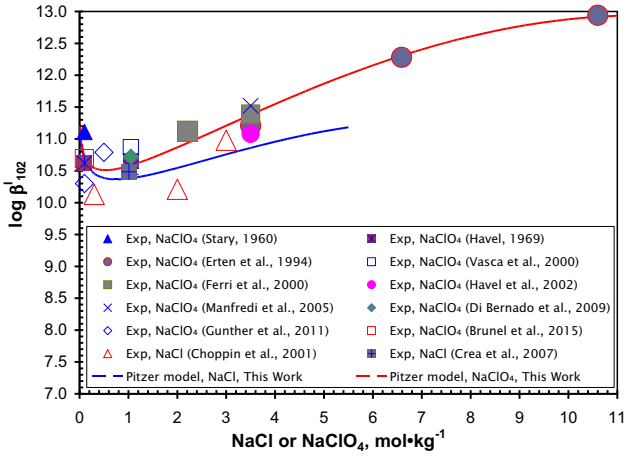


Figure 2: Comparison of the stability constants for $UO_2(C_2O_4)_2^{2-}$ as a function of ionic strength in NaCl and $NaClO_4$ media predicted by the model with the experimental data.

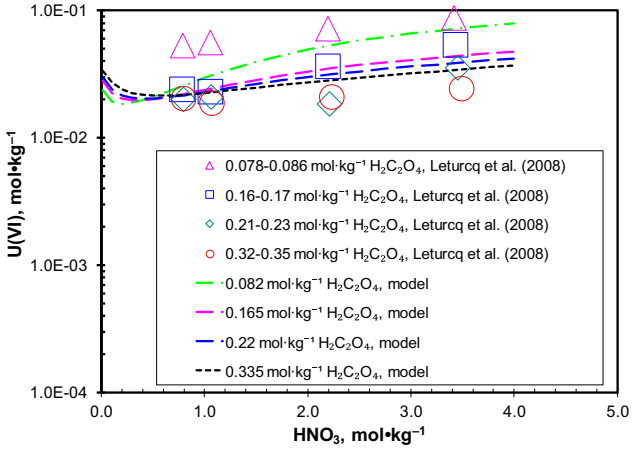


Figure 3: Comparison of the solubility of $UO_2C_2O_4$•$3H_2O$(cr) in the mixtures of oxalic and nitric acids predicted by the model with the experimental data.

we also use the method of [35, 36] for the prediction of densities of mixtures based on the densities of pure constituent components. The densities for pure $H_2C_2O_4$ and HNO_3 are taken from [34, 37], respectively. Figure 3 shows that the model reproduces the experimental data reasonably well, particularly in the high ionic strength range.

Table 3 lists the equilibrium constants for $UO_2C_2O_4$(aq), $UO_2(C_2O_4)_2^{2-}$, and $UO_2C_2O_4$•$3H_2O$(cr) in our model in comparison with those of Hummel et al. [6]. Our value for $\log_{10}\beta^0_{101}$ is 7.54 ± 0.30 in comparison with a value of 7.13 ± 0.16 from Hummel et al. [6], suggesting that $UO_2C_2O_4$(aq) is slightly stronger in our model than that advanced by Hummel et al. [6]; note that the values agree with each other within the reported uncertainties. It should also be noted that our model considers all the data given by Erten et al. [24]. In that study, Erten et al. [24] provides experimental data at I = 3, 5, 7, and 9 mol•dm^{-3} in $NaClO_4$ solutions. In the model of Hummel et al. [6], the authors used data only at I = 3 mol•dm^{-3} $NaClO_4$ from Erten et al. [24] because the other ionic strengths exceeds the applicable range of the SIT model. Therefore, the difference of our model from Hummel et al. [6] for $UO_2C_2O_4$(aq) can be attributed to the different data that the two models use.

Regarding $\log_{10}\beta^0_{102}$ for $UO_2(C_2O_4)_2^{2-}$, our model has a value of 11.57 ± 0.20, which agrees with the value of 11.65 ± 0.15 in Hummel et al. [6].

With regard to $\log_{10}K^0_{sp}$ for $UO_2C_2O_4$•$3H_2O$(cr), our model has a value of –9.36 ± 0.25 in comparison with a value of –8.93 ± 0.31 reported in Hummel et al. [6]. In our model, we utilize the more recent data from Leturcq et al. [33]; published after Hummel et al. [6]. Our $\log_{10}K^0_{sp}$ value is slightly more negative than that given in Hummel et al. [6] when considering the uncertainty ranges of these values.

We have performed the validation tests for our model by using experimental data not used in our model development. In the first validation test, we compared the model-predicted solubilities of $UO_2C_2O_4$•$3H_2O$(cr) in HNO_3 solutions with experimental data from [38–41]. Figure 4 demonstrates that the model-predicted values are in good

Table 3: Comparison of the equilibrium constants for uranyl-oxalate species in molal unit at infinite dilution and 25 °C obtained in this work with those in the NEA review.

Equilibrium constant	Pitzer model, this work	SIT model [6]
$\log_{10}\beta^0_{101}$ for $UO_2C_2O_4$(aq)	7.54 ± 0.30	7.13 ± 0.16
$\log_{10}\beta^0_{102}$ for $UO_2(C_2O_4)_2^{2-}$	11.57 ± 0.20	11.65 ± 0.15
$\log_{10}K^0_{sp}$ for $UO_2C_2O_4$•$3H_2O$(cr)	–9.36 ± 0.25	–8.93 ± 0.31

agreement with the independent experimental data over a wide range of ionic strengths from dilute to ~5 mol•kg^{-1}.

In the second validation test, we compare the model-predicted solubilities of $UO_2C_2O_4$•$3H_2O$(cr) in the mixture of HNO_3 and $UO_2(NO_3)_3$ with the experimental data at 25 °C from [42]. In the experiments of Pimentel and Stevenson [42], the equilibrium was approached from both supersaturation and undersaturation. The concentrations of HNO_3 range from 0.5 to 2 mol•dm^{-3}, and $UO_2(NO_3)_3$ range from 0.24 to 0.99 mol•dm^{-3}. The concentrations in molarity units for the mixture of HNO_3 and $UO_2(NO_3)_3$ are converted to those in molality units following the same method for the mixtures of HNO_3 and $NaNO_3$, and of $H_2C_2O_4$ and HNO_3 described above. Figure 5 indicates the model-predicted values are in good agreement with the independent experimental data.

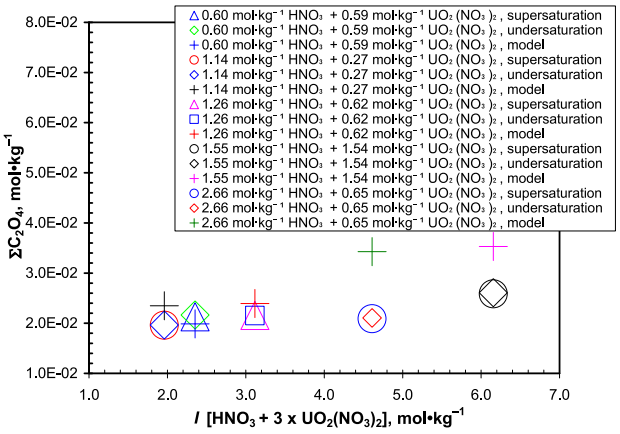


Figure 5: Model-predicted solubilities of $UO_2C_2O_4$•$3H_2O$(cr) expressed as concentrations of total oxalate as function of ionic strength in the mixtures of HNO_3 and $UO_2(NO_3)_2$, in comparison with the experimental data. The experimental data are from Pimentel and Stevenson (1945) [42]. All experimental data are independent of the model developed in this study. The experimental data are represented by unfilled symbols, and all of model-predicted values are represented by cross symbols.

4 Applications

As an example for model applications, we calculate the speciation of uranyl species as a function of pH_m in solutions with different ionic strengths. The solutions that we select include 0.1 mol•kg^{-1} NaCl (I = 0.1 mol•kg^{-1}), ERDA-6 brine (I = 5.82 mol•kg^{-1}), and GWB (I = 8.26 mol•kg^{-1}). The 0.1 mol•kg^{-1} NaCl could represent the dilute groundwaters in the disposal concept in granite and crystalline rocks. The ERDA-6 and GWB are from the WIPP site [9], and can represent groundwaters in salt formations and sedimentary basins. We assume that the total oxalate concentrations are in the order of 1.7×10^{-2} mol•dm^{-3}, a value taken from [4] for the WIPP Compliance Recertification

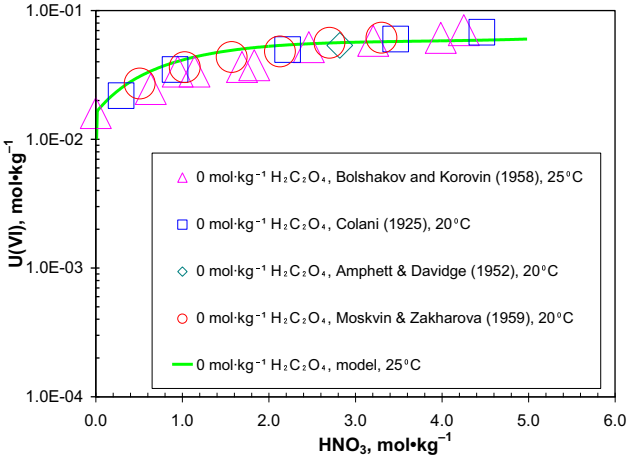


Figure 4: Comparison of the solubility of $UO_2C_2O_4$•$3H_2O$(cr) in nitric acid predicted by the model with the experimental data. All experimental data are independent of the model developed in this study.

Application Performance Assessment in 2009. The total uranyl concentrations are assumed to be in the order of 10^{-3} mol•dm^{-3}, a value used for the WIPP Compliance Recertification Applications Performance Assessment in 2009 and 2014.

Figure 6 displays our calculations in 0.1 mol•kg^{-1} NaCl. In these calculations, we include monomeric uranyl hydroxyl and carbonate complexes as well as UO_2^{2+}, $UO_2(C_2O_4)$(aq), and $UO_2(C_2O_4)_2^{2-}$. The stability constants for monomeric uranyl hydroxyl and carbonate complexes are taken from [43] without consideration of the specific interactions, as the specific interaction effects are negligible at I = 0.1 mol•kg^{-1}. The total carbonate concentrations are assumed to be at a value of 9×10^{-4} mol•kg^{-1} over the entire pH_m range. This value is the value controlled by the equilibrium assemblage of brucite and hydromagnesite [44] at pH_m 10. Figure 6 shows that $UO_2(C_2O_4)$(aq) and $UO_2(C_2O_4)_2^{2-}$ are the dominant species up to pH_m ~9.4. Above pH_m ~9.4, uranyl hydroxyl complexes become dominant. Uranyl carbonate complex, $UO_2(CO_3)_3^{4-}$, becomes a significant, but not a dominant, species starting from pH_m 7.6 (i.e., contributions ≥10%).

In our calculations at high ionic strengths (e.g., GWB and ERDA-6), the other uranyl species except UO_2^{2+} are omitted based on the following reasoning. First, the strengths of the uranyl complexes with most of inorganic ligands are weaker than those of uranyl oxalate species. The strengths of uranyl complexes with hydroxyl ion and carbonate [44] are comparable to those of uranyl oxalate

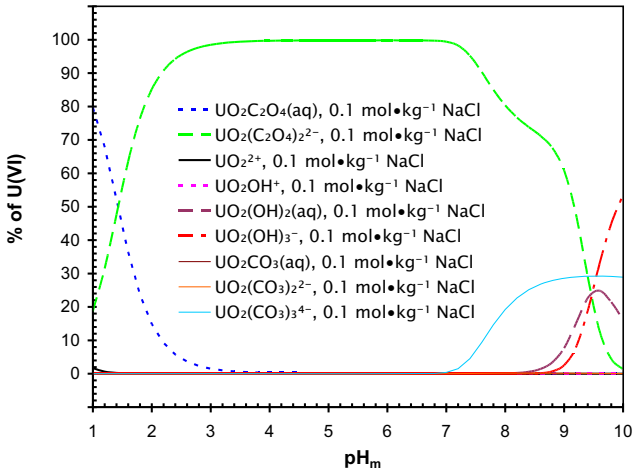


Figure 6: Distributions of uranyl oxalate species as a function of hydrogen ion concentrations on a molal scale (pH_m) in 0.1 m NaCl. The calculations were performed by assuming $\Sigma C_2O_4 = 1.7 \times 10^{-2}$ mol•dm^{-3} and $\Sigma U(VI) = 10^{-3}$ mol•dm^{-3}, using the oxalate concentrations for the WIPP 2009 PABC (Brush and Xiong, 2009 [3]) as an example. The carbonate concentration is assumed to controlled by the assemblage of brucite and synthetic hydromagnesite, which has a CO_2(g) fugacity of $10^{-6.13\pm0.16}$ bars [44]. Precipitation is suppressed.

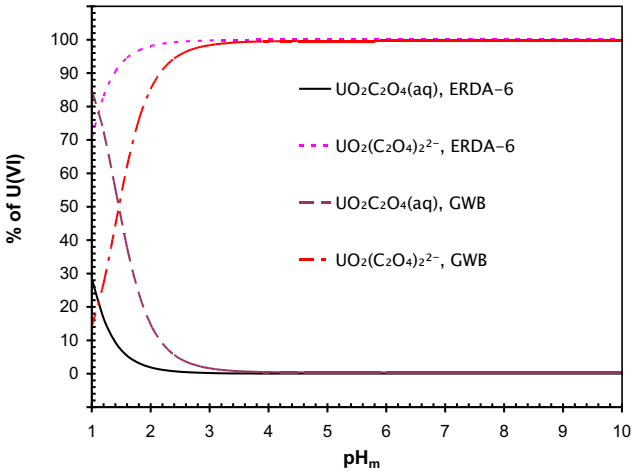


Figure 7: Distributions of uranyl oxalate species as a function of hydrogen ion concentrations on a molal scale (pH_m) in different solutions with various ionic strengths. The calculations were performed by assuming $\Sigma C_2O_4 = 1.7 \times 10^{-2}$ mol•dm^{-3} and $\Sigma U(VI) = 10^{-3}$ mol•dm^{-3}, using the oxalate concentrations for the WIPP 2009 PABC [3]. As the contributions from UO_2^{2+} are generally less than 1%, they are omitted for simplicity. Solid precipitation is suppressed.

species, but the oxalate concentrations that we adopt are much higher than those of hydroxyl ion and carbonate concentrations. Finally, the Pitzer model for the uranyl complexes with other ligands such as hydroxide and carbonate has not been established yet, and therefore the direct comparisons are not feasible at present.

Figure 7 shows that $UO_2(C_2O_4)_2^{2-}$ is the dominant species above pH_m ~2 in all solutions with different ionic strengths. The compositions for ERDA-6 and GWB used for the calculations are presented in Table 4. In the low pH_m range, there are some differences between ERDA-6 and GWB with regard to the speciation distribution. In ERDA-6, the percentage of $UO_2C_2O_4$(aq) is much less than that in GWB.

In addition, the interactions of U(VI) with oxalate in the far field of a geological repository are also expected to be important, should U(VI) be leaked from a breached geological repository. This is because oxalate is ubiquitous in the surface of the Earth, and whewellite is quite common in various geological environments [46–49], serving as a major source for oxalate in the far field. The presence of whewellite in the uranium deposits (e.g., [46, 49]) and the formation of the natural uranyl oxalate minerals such as uroxite ($[(UO_2)_2(C_2O_4)(OH)_2(H_2O)_2]$•$H_2O$) and metauroxite ($[(UO_2)_2(C_2O_4)(OH)_2(H_2O)_2]$) [50] provide the clues about the interactions of U(VI) with oxalate in the far field of a geological repository.

Table 4: Chemical compositions of the brines with high ionic strengths employed for the calculations of the uranyl oxalate species*.

Total elemental concentration	GWB (Generic Weep Brine), mol•kg^{-1}	ERDA-6 (Energy Research Development Administration Well 6), mol•kg^{-1}
Na^+	3.98	5.44
K^+	0.526	0.109
Li^+	5.05×10^{-3}	None
Ca^{2+}	1.56×10^{-2}	1.34×10^{-2}
Mg^{2+}	1.15	2.13×10^{-2}
Cl^-	6.32	5.20
Br^-	3.00×10^{-2}	1.23×10^{-2}
SO_4^{2-}	0.200	0.187
$B_4O_7^{2-}$	4.45×10^{-2}	1.76×10^{-2}

*From [45].

5 Conclusion

In this study, we have developed a thermodynamic model with Pitzer formalism for the system of UO_2^{2+}–Na^+–H^+–Cl^-–ClO_4^-–$C_2O_4^{2-}$–NO_3^-–H_2O system at 25 °C, up to the ionic strength of ~11 mol•kg^{-1}. Our model is validated against the independent solubility data of $UO_2C_2O_4$•$3H_2O$(cr) in HNO_3 solutions and the mixtures of HNO_3 and $UO_2(NO_3)_2$ at 20–25 °C. The model can be applied to the investigations of the interactions of U(VI) with oxalate in the near field for the

disposal concepts over a wide range of ionic strengths such as nuclear waste disposals in crystalline rocks, clay formations, salt formations and sedimentary basins. It can be applied to many industrial processes with high ionic strengths related to nuclear materials including spent fuel reprocessing, and the treatment of high level nuclear waste. In addition, the model can also be applied to modeling the interactions of U(VI) with oxalate in the far field of a geological repository.

Acknowledgements: Sandia National Laboratories is a multi-mission laboratory operated by National Technology and Engineering Solutions of Sandia, LLC., a wholly owned subsidiary of Honeywell International, Inc., for the U.S. Department of Energy's National Nuclear Security Administration under contract DE-NA-0003525. This paper is published with the release number of SAND2020-14126J. This research is funded by the Spent Fuel and Waste Science and Technology (SFWST) programs administered by the Office of Nuclear Energy (NE) of the U.S. Department of Energy. This paper describes objective technical results and analysis. Any subjective views or opinions that might be expressed in the paper do not necessarily represent the views of the U.S. Department of Energy or the United States Government. We thank journal reviewers for the insightful and thorough reviews, which helped to improve our manuscript.

Author contributions: All the authors have accepted responsibility for the entire content of this submitted manuscript and approved submission.

Research funding: None declared.

Conflict of interest statement: The authors declare no conflicts of interest regarding this article.

References

1. Ferri D., Iuliano M., Manfredi C., Vasca E., Caruso T., Clemente M., Fontanella C. Dioxouranium (VI) oxalate complexes. *J. Chem. Soc, Dalton Trans.* 2000, *19*, 3460.
2. Wolff-Boenisch D., Traina S. J. The effect of desferrioxamine B, enterobactin, oxalic acid, and Na-alginate on the dissolution of uranyl-treated goethite at pH 6 and 25 °C. *Chem. Geol.* 2007, *243*, 357.
3. Brush L. H., Xiong Y.-L. *Calculation of Organic-Ligands Concentrations for the WIPP CRA-2009 PABC*; Analysis Report: Sandia National Laboratories, Carlsbad, NM, 2009. ERMS 551481.
4. Brush L. H., Domski P. S. *Calculation of Organic Ligand Concentrations for the WIPP CRA-2014 PA*; Analysis Report: Sandia National Laboratories, Carlsbad, NM, 2013.
5. Berton A., Jacquemet N., Erable B., Sablayrolles C., Escadeillas G., Albrecht A. Reactivity of nitrate and organic acids at the concrete-bitumen interface of a nuclear waste repository cell. *Nucl. Eng. Des.* 2014, *268*, 51.
6. Hummel W., Anderegg G., Puigdoménech I., Rao L., Tochiyama O. Chemical thermodynamics of compounds and complexes of U, Np, Pu, Am, Tc, Se, Ni and Zr with selected organic ligands. In *Chemical Thermodynamics Series*; OECDNEA, Ed., Vol. *9,* 2005.
7. Hummel W., Puigdomènech I., Rao L., Tochiyama O. Thermodynamic data of compounds and complexes of U, Np, Pu and Am with selected organic ligands. *Compt. Rendus Chem.* 2007, *10*, 948.
8. Hobbs D. T. *Impacts of Sodium Oxalate on High-Level Waste Processing at the Savannah River Site*; WSRC-TR-2003-00120: Westinghouse Savannah River Company, Savannah River Site, Aiken, SC 29808, USA, 2003.
9. Xiong Y.-L., Lord A. C. S. Experimental investigations of the reaction path in the $MgO–CO_2–H_2O$ system in solutions with ionic strengths, and their applications to nuclear waste isolation. *Appl. Geochem.* 2008, *23*, 1634.
10. Hobbs M. Y., Frape S. K., Shouakar-Stash O., Kennell L. R. *Phase I Regional Hydrogeochemistry, Southern Ontario: OPG's Deep Geologic Repository for Low & Intermediate Level Waste*; Supporting Technical Report OPG 00216-REP-01300-00006-R00, Ontario Power Generation: Canada, Toronto, 2008.
11. Zabunoglu O. H., Ozdemir L. Purex co-processing of spent LWR fuels: flow sheet. *Ann. Nucl. Energy* 2005, *32*, 151.
12. Wolery T. J., Xiong Y.-L., Long J. *Verification and Validation Plan/ Validation Document for EQ3/6 Version 8.0a for Actinide Chemistry, Document Version 8.10*; Sandia National Laboratories: Carlsbad, NM. ERMS 550239, 2010.
13. Xiong Y.-L. *WIPP Verification and Validation Plan/Validation Document for EQ3/6 Version 8.0a for Actinide Chemistry, Revision 1, Document Version 8.20. Supersedes ERMS 550239*; Sandia National Laboratories: Carlsbad, NM. ERMS 555358, 2011.
14. Xiong Y.-L. A thermodynamic model for silica and aluminum in alkaline solutions with high ionic strength at elevated temperatures up to 100 °C: applications to zeolites. *Am. Mineral.* 2013, *98*, 141.
15. Xiong Y.-L. A pitzer model for the $Na–Al(OH)_4–Cl–OH$ system and solubility of boehmite (AlOOH) to high ionic strength and to 250 °C. *Chem. Geol.* 2014, *373*, 37.
16. Xiong Y.-L. Experimental determination of lead carbonate solubility at high ionic strengths: a Pitzer model description. *Monatsh. Chem.* 2015, *146*, 1433.
17. Thakur P., Xiong Y.-L., Borkowski M. An improved thermodynamic model for the complexation of trivalent actinides and lanthanide with oxalic acid valid to high ionic strength. *Chem. Geol.* 2015, *413*, 7.
18. Pitzer K. S. Theory: ion interaction approach. In *Activity Coefficients in Electrolyte Solutions*; Pytkowicz R. M., Ed. CRC Press: Boca Raton, FL, 1979; pp. 157–208.
19. Pitzer K. S. *Ion Interaction Approach: Theory and Data Correlation. Activity Coefficients in Electrolyte Solutions*, 2nd ed. CRC Press: Boca Raton, Florida, 1991; pp. 75–153.
20. Starý J. Bestimmung der Zusammensetzung und der Stabilitätskonstanten von Metallkomplexen durch Extraktionsmethode. *Collect. Czech Chem. Commun.* 1960, *25*, 2630.
21. Havel J. Spectrophotometric study of complex formation of uranyl with oxalic acid. *Collect. Czech Chem. Commun.* 1969, *34*, 3248.
22. Choppin G. R., Bokelund H., Valkiers S. Oxalate complexation in dissolved carbide systems. *Radiochim. Acta* 1983, *33*, 229.

23. Van Loon L. R., Kopajtic Z. Complexation of Cu^{2+}, Ni^{2+} and UO_2^{2+} by radiolytic degradation products of bitumen. *Radiochim. Acta* 1991, *54*, 193.
24. Erten H. N., Mohammed A. K., Choppin G. R. Variation of stability constants of thorium and uranium oxalate complexes with ionic strength. *Radiochim. Acta* 1994, *66*, 123.
25. Vasca E., Caruso T., Iuliano M., Manfredi C., Fontanella C., Trifuoggi M. Studies on metal oxalate complexes. I. Validation of the reversibility of the Hg, $Hg_2C_2O_4$ (s) electrochemical couple. *Ann. Chim.* 2000, *90*, 181.
26. Choppin G. R., Bond A. H., Borkowski M., Bronikowski M. G., Chen J.-F., Lis S., Mizera J., Pokrovsky O. S., Wall N. A., Xia Y.-X., Moore R. C. *Waste Isolation Pilot Plant Actinide Source Term Test Program: Solubility Studies and Development of Modeling Parameters*; Report. SAND99-0943: Sandia National Laboratories: Albuquerque, New Mexico, USA, 2001.
27. Havel J., Soto-Guerrero J., Lubal P. Spectrophotometric study of uranyl–oxalate complexation in solution. *Polyhedron* 2002, *21*, 1411.
28. Manfredi C., Ferri D., Vasca E., Caruso T., Caruso V., Fontanella C., Palladino G., Vero S. On the hydrolysis of the dioxouranium (VI) ion in oxalate solutions. *Ann. Chim.* 2005, *95*, 313.
29. Crea F., De Robertis A., De Stefano C., Sammartano S. Dioxouranium (VI)–carboxylate complexes: a calorimetric and potentiometric investigation of interaction with oxalate at infinite dilution and in NaCl aqueous solution at I = 1.0 mol L^{-1} and T = 25 °C. *Talanta* 2007, *71*, 948.
30. Di Bernardo P., Zanonato P. L., Tian G., Tolazzi M., Rao L. Thermodynamics of the complexation of uranium (VI) with oxalate in aqueous solution at 10–70 °C. *Dalton Trans.* 2009, *23*, 4450.
31. Günther A., Steudtner R., Schmeide K., Bernhard G. Luminescence properties of uranium (VI) citrate and uranium (VI) oxalate species and their application in the determination of complex formation constants. *Radiochim. Acta* 2011, *99*, 535.
32. Brunel B., Philippini V., Mendes M., Aupiais J. Actinide oxalate complexes formation as a function of temperature by capillary electrophoresis coupled with inductively coupled plasma mass spectrometry. *Radiochim. Acta* 2015, *103*, 27.
33. Leturcq G., Costenoble S., Grandjean S. *Uranyl Oxalate Solubility*; ATALANTE 2008: French Atomic Energy Commission (CEA), Paris-Saclay: Montpellier, France, 2008.
34. Söhnel O., Novotný P. *Densities of Aqueous Solutions of Inorganic Substances*; Elsevier: Amsterdam, 1985; p. 335.
35. Patwardhan V. S., Kumar A. A unified approach for prediction of thermodynamic properties of aqueous mixed-electrolyte solutions. Part I. Vapor pressure and heat of vaporization. *AIChE J.* 1986, *32*, 1419.
36. Patwardhan V. S., Kumar A. A unified approach for prediction of thermodynamic properties of aqueous mixed-electrolyte solutions. Part II. Volume, thermal, and other properties. *AIChE J.* 1986, *32*, 1429.
37. Kandpal K., Joshi B. K., Joshi S. K., Kandpal N. D. Interaction studies of dilute aqueous oxalic acid. *E-J. Chem.* 2007, *4*, 574.
38. Colani A. Etude de l'oxalate d'uranyle. *Bull. Soc. Chim. Fr. Mem.* 1925, 856.
39. Amphlett C. B., Davidge O. T. The solubility of uranyl oxalate in nitric acid. *J. Chem. Soc.* 1952, 2938.
40. Bolshakov K. A., Korovin S. S. *Tr. Inst.-Mosk. Inst. Tonkoi Khim.-Tekhnol. im. M. V. Lomonosova* 1958, *7*, 165.
41. Moskvin A. I., Zakharova F. A. Investigation of the formation of uranyl complexes in oxalate solutions by the solubility method. *Russ. J. Inorg. Chem.* 1959, *4*, 975.
42. Pimentel G. C., Stevenson F. R. *The Solubility of Uranyl Oxalate and the Existence of Undissociated Uranyl Oxalate in Solution*; AECD-2323: U.S. Atomic Energy Commission (AEC): Washington, D.C., 1945.
43. Guillaumont R., Fanghänel T., Fuger J., Mompean F. J., Grenthe I., Neck V., Palmer D. A., Rand M. H. *Update on the Chemical Thermodynamics of Uranium, Neptunium, Plutonium Americium and Technetium. Chemical Thermodynamics*, Vol. *5*, Elsevier: Amsterdam, 2003; p. 919.
44. Xiong Y.-L. Experimental determination of solubility constant of hydromagnesite (5424) in NaCl solutions up to 4.4 m at room temperature. *Chem. Geol.* 2011, *284*, 262.
45. Xiong Y.-L. *Activity/Project Specific Procedure: SP 20-4 Preparing Synthetic Brines for Geochemical Experiments, Revision 2*; Sandia National Laboratories: Carlsbad, NM, 2008. https://nwmp.sandia.gov/onlinedocuments/nwmp/sp/sp2004.pdf.
46. Gude A. J. 3rd, Young E. J., Kennedy V. C., Riley L. B. Whewellite and celestine from a fault opening in San Juan County, Utah. *Am. Mineral.* 1960, *45*, 1257.
47. Stephens W. E. Whewellite and its key role in living system. *Geol. Today* 2012, *28*, 180.
48. Hofmann B., Bernasconi S. M. Review of occurrences and carbon isotope geochemistry of oxalate minerals: implications for the origin and fate of oxalate in diagenetic and hydrothermal fluids. *Chem. Geol.* 1998, *149*, 127.
49. Knizek F., Litochleb J. Calcite druse cavities with whewellite on the Bytiz uranium deposit (the Pribram uranium-polymetallic district, Central Bohemia). *Bull. Mineralogicko-Petrologického Oddělení Národního Muzea V. Praze* 2005, *13*, 73.
50. Kampf A. R., Plášil J., Nash B. P., Němec I., Marty J. Uroxite and metauroxite, the first two uranyl oxalate minerals. *Mineral. Mag.* 2020, *84*, 131.